Asynchronous bubble pinch-off pattern arising in fluidized beds due to jet interaction: A magnetic resonance imaging and computational modeling study

A. Penn [ID],[1,2,*] A. Padash [ID],[3,*] M. Lehnert,[1] K. P. Pruessmann,[2] C. R. Müller,[1,†]
and C. M. Boyce [ID][3,‡]

[1]*Department of Mechanical and Process Engineering, ETH Zurich, CH-8092 Zurich, Switzerland*
[2]*Institute for Biomedical Engineering, ETH Zurich and University of Zurich, CH-8092 Zurich, Switzerland*
[3]*Department of Chemical Engineering, Columbia University, New York, New York 10027, USA*

Rapid magnetic resonance imaging is used to study the interaction between two gas jets injected into a 3D incipiently fluidized bed. At large separation distances and in cases with larger particles, bubbles pinch off from the two jets simultaneously with one another. At small separation distances with smaller particles, a jet grows at one orifice while a jet pinches off to form a bubble at the other orifice, resulting in bubbles pinching off the two jets nearly completely out-of-phase from one another. Discrete particle simulations coupled with computational fluid dynamics reproduce these two patterns. Simulations demonstrate that the asynchronous pattern emerges due to drag forces on the particles causing particle inertia dominate dissipation, causing motion of particles between the jets to become unstable. Specifically, when one jet is growing, it forces particles to move toward the neighboring jet, causing a bubble to break off from the neighboring jet.

I. INTRODUCTION

Fluidized beds are formed when upward gas flow through a bed of granular particles suspends the particles, causing them to exhibit properties resembling those of a continuous liquid, rather than a set of discrete solid particles. Fluidized beds have been the subject of decades of research in the engineering and physics communities due to both their relevance to a variety of industrial processes as well as their intriguing physical aspects which blend solid, liquid, and gaseous physics. The entry of gas into fluidized beds often comes in the form of jets: concentrated areas of gas flow through an orifice which can form permanent voids as well as voids which oscillate in space and time as bubbles of gas pinch off from these voids and subsequently rise to the bed surface. These jets are of industrial importance since they affect the gas-solid contact and solids mixing in industrial processes. Jets are also interesting on a fundamental physics basis, since their behavior is in many ways analogous to jets and plumes in gas-liquid systems, despite the fact that no surface tension exists between gaseous voids and particulate regions in fluidized beds and thus gas passes freely between voids and the interstices between particles.

Previous experimental [1–5] and numerical [3,5–7] studies have investigated the interaction between two jets in fluidized beds. These studies have generally noted three regimes of behavior

---

*These authors contributed equally to the work.

†muelchri@ethz.ch

‡cmb2302@columbia.edu

[1,2,6,7]: (1) an isolated regime in which the two jets do not affect one another, (2) a coalesced or merged regime in which the jets or the bubbles which pinch off from them merge into a single body, and (3) a transition regime in between the isolated and coalesced regime. These studies have noted that the strongest factor differentiating these regimes is the separation distance between orifices and that gas jet velocity acts as a secondary factor. The largest difference between previous studies has been the description of the transition regime: descriptions have included (a) jets looking essentially like isolated jets but taller due to jet-jet interaction [1], (b) jets and bubbles changing in shape due to one another but not coalescing [6,7], and (c) jets oscillating in time between acting as isolated jets and coalescing [2]. An issue with these previous studies has been that they have characterized jet interaction in pseudo-2D beds or semicylindrical beds where the jets are located near the planar wall to enable optical measurements. Since jets also have been shown to interact with walls [8], it is unclear how wall effects could impact the understanding of jet interaction provided by the prior work.

Here, we seek to use rapid magnetic resonance imaging (MRI) of particle concentration and velocity in a 3D fluidized bed as well as computational fluid dynamics—discrete element method (CFD-DEM) simulations to provide new insights into the transition regime of bubble interaction in fluidized beds. Several previous studies have used tomographic imaging, such as x-ray and MRI, to study the internal dynamics of fluidized beds [9,10]. Two excellent review articles provide an overview of MRI of granular materials and flow phenomena [11,12]. Notably, prior studies have used MRI to investigate jetting in fluidized beds [8,13–15]. However, these studies mostly have been limited to time-averaged measurements [8,14], and thus have not been able to image the dynamics of interacting jets in the transitional regime. Additionally, they have often studied systems where the only gas flow came from the jet orifices [8,13,14], and thus gas from jets was used to both fluidize the bed and generate a jet, leading to very different dynamics from studies in which background gas flow from the distributor fluidizes the particles [15]. One study [15] achieved rapid MRI of jet and bubble motion in a system with a central jet and background gas flow; however, the imaging was not able to produce rapid images of particle velocity and only one jet was studied, precluding understanding of dynamic jet interaction. Recently developed MRI advances [16] have enabled dynamic imaging of both particle concentration and velocity, and these capabilities have been used to characterize bubble dynamics in beds with [17] and without [18,19] cohesive liquid bridging. These techniques have also recently been used to characterize the dynamics of single jets injected into incipiently fluidized beds [20,21]. Here, we use these rapid MRI techniques and simulations to enable us to identify new types of behavior in the transitional jet interaction regime and describe the underlying physical mechanisms.

II. METHODS

A. Fluidized bed

The fluidized bed was made of polymethyl methacrylate (PMMA) and was cylindrical with an inner diameter of 190 mm and a height of 300 mm. It was filled with particles to a height $H_0 = 200$ mm; the particles were agar shells filled with middle-chain triglyceride oil from which MRI signal was derived. Two different sizes of particles were used in separate experiments: (1) "1-mm particles," which had a diameter $d_p = 1.02 \pm 0.12$ mm, a density $\rho_p = 1040$ kg/m³, a coefficient of friction $\mu = 0.54 \pm 0.05$, and a coefficient of restitution $e = 0.70 \pm 0.03$, and (2) "3-mm particles," with $d_p = 2.93 \pm 0.04$ mm, $\rho_p = 1040$ kg/m³, $\mu = 0.56 \pm 0.04$, and $e = 0.69 \pm 0.03$. Air at ambient conditions flowed through a distributor made from a 10-mm perforated plate of PMMA to fluidize the particles. Particle with a diameter of 3 mm falls into Geldart [22] Group D and 1-mm particles are on the border between Groups B and D. The minimum fluidization velocities of the 1- and 3-mm particles were 0.25 and 0.70 m/s, respectively.

For both types of particles, the coefficients of restitution were measured by dropping individual particles from 130 mm height onto a polished horizontal stone surface and recording the rebound height of the particles with a high speed camera. The measurements were repeated ten times in

order to obtain the coefficients of restitution and their standard deviation. The described technique neglects the effect of the air resistance and therefore the actual coefficients of restitution might be slightly higher compared to the reported values. The angles of repose θ_r were measured by filling a transparent horizontal cylinder of diameter 100 mm halfway with particles and slowly rotating the cylinder around its axis at about 0.2 rpm, while recording the inclination angle between the particle surface and a horizontal level using a camera. The coefficient of friction μ was determined according to $\mu = \tan(\theta_r)$.

B. Jet and bubble injection

Gas was injected through orifices which were flush with the distributor and $d_o = 7.95$ mm in diameter. Three different configurations of orifices were used: (1) a single central port, (2) two ports with centers separated by $d_{sep} = 40$ mm, each 20 mm from the center of the distributor, corresponding to $d_{sep}/d_o = 5.0$ and (3) two ports separated by $d_{sep} = 80$ mm, each 40 mm from the center, corresponding to $d_{sep}/d_o = 10.1$. For jet injection, gas was injected continuously from a 2.5 L tank kept at constant pressure; the pressure of the tank was set to different values to achieve different flow rates of gas through the jets, corresponding to different average gas velocities through the jet orifices (u_{jet}). For all cases, the flow rates through both jets in one experiment were the same.

C. MRI measurements

MRI measurements were conducted by surrounding the fluidized bed with a custom-built 16-channel radiofrequency array [16] and placing the system in a Philips Achieva 3T medical scanner. Both the solids volume fraction and the vertical and horizontal components of the particle velocity were measured simultaneously using echo planar imaging (EPI) [23] with phase contrast velocimetry [24]. The temporal resolution of the measurements was 18 ms, the nominal spatial resolution was 3 mm horizontal (x)×5 mm vertical (y), and the field-of-view was 200 mm (x)×300 mm (y). Images were taken of a central vertical slice through the bed with a slice thickness of 10 mm. The MRI pulse sequence and methods used are described further by Penn *et al.* [16]. In processing of the MRI velocity images, pixels which contained a particle signal intensity less than 25% of the maximum intensity were considered as consisting of the gas phase. The particle velocities were set to zero in the gas-phase pixels to avoid the images from showing spurious low signal-to-noise particle velocity measurements in these gas-laden regions.

D. Numerical simulations

CFD-DEM simulations were conducted in a 3D cylindrical bed with an inner diameter of 190 mm and a height of 300 mm matching the size of the experimental setup. The simulations used CFD to model the gas flow on a computational grid and DEM was used to model the motion of each individual particle using Newtonian and contact mechanics. Simulations were conducted using the open source CFDEMCoupling software [25] which combines CFD from OpenFOAM [26,27] and DEM from LIGGGHTS. A prior paper provides the full equations used [28].

The simulations matched the particle properties used in the experiments. The minimum fluidization velocity measured in the simulations for the 1- and 3-mm particles were 0.25 and 0.70 m/s, respectively, matching those determined experimentally. To match the cylindrical experimental geometry, an unstructured grid with rectangular cells was used in the center of the system and wedge-shaped cells near the walls. Figure 1 shows a horizontal cross section of the mesh used in CFD for (a) 1-mm particles and (b) 3-mm particles. For 1-mm particles, the grid spacing in the vertical-direction was $dz = 3$ mm, and for the square grid cells far from the boundaries $dx = dy = 3.015$ mm was used in the horizontal direction. For 3-mm particles, $dz = 9.375$ mm, and $dx = dy = 9.047$ mm were used. Grid sizes were chosen to be approximately three times the particle diameter to match that the recommended values for CFD-DEM simulations in the literature [29]. The jet injection ports were square in shape with side length of 9.05 mm, and they were
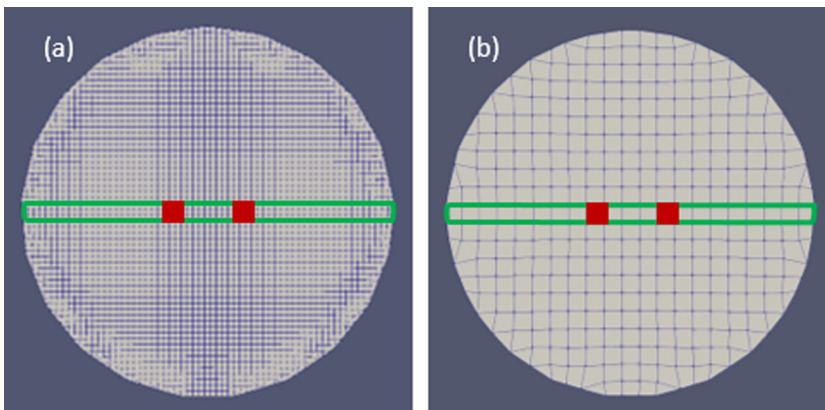
FIG. 1. Horizontal cross-section view of the fluid grid used for (a) 1-mm particles and (b) 3-mm particles, with the green slice showing CFD cells used in vertical cross-section images and the red squares showing the two ports for jet injection at the gas distributor.

separated by $d_{sep} = 36.2$ mm, each 18.1 mm from the center of the grid, corresponding to the experiment in which the ports are separated by 40 mm. An incompressible code with an implicit solver was used with CFD time step of 0.1 ms. The no-slip wall boundary condition as well as constant pressure for the outlet boundary condition were used for CFD. In DEM, the Poisson's ratio and Young's modulus used were 0.32 and 10 MPa, respectively with a time step of 0.001 ms. The two phases were coupled using Wen and Yu drag law [30]. Jet velocities used in simulations were significantly different from those used in experiments, as has been seen in simulations for bubble injection [31]. These differences can be attributed to (i) inaccuracies in the measurement of jet velocity and (ii) inaccuracies in the drag law used in simulations. The sources of this difference in jet velocity to produce similar results is worthy of a complete study, but we consider this outside of the scope of the current study.

III. RESULTS

A. MRI results

Figure 2 shows a time series of images of particle concentration (upper row) and particle velocity (lower row) taken of a central vertical slice through the fluidized bed. The images are of two gas jets injected into the bed of 1-mm particles with a separation distance of $d_{sep}/d_o = 5.0$ between the center of jets with gas velocities through the jet orifices of $u_{jet} = $ (a) 38 m/s, (b) 66 m/s and (c) 97 m/s. For all cases, vertical jets form just above the orifices and the jets pinch off to form bubbles which rise to the bed surface. Particle velocities are fast and upward surrounding the jets and bubbles and slow and downward in the outer annulus of the bed. In all cases, an asynchronous bubbling pattern is observed: When a jet is growing on the right side, a jet pinches off into a bubble on the left side and vice versa. Bubble pinch-off from the two jets is approximately $180°$ out-of-phase. This forms an alternating pattern of bubbles which rises in a pattern that resembles interlocking teeth in a zipper, until the pattern is broken by bubbles coalescing. With increasing gas flow rate, the jets become larger before pinching off to form bubbles, resulting in larger bubbles rising through the bed.

Figure 3 shows a time series of images of particle concentration and velocity for a single central gas jet injected into an incipiently fluidized bed of 1-mm particles with a gas velocity through the jet orifice $u_{jet} = 52$ m/s. Vertical bulbous gas jets form directly above the orifice, and these jets pinch off to form bubbles which rise to the bed surface without coalescing. Particle velocities are high and upward directly above and below jets and bubbles, but move downward slowly to the sides of the
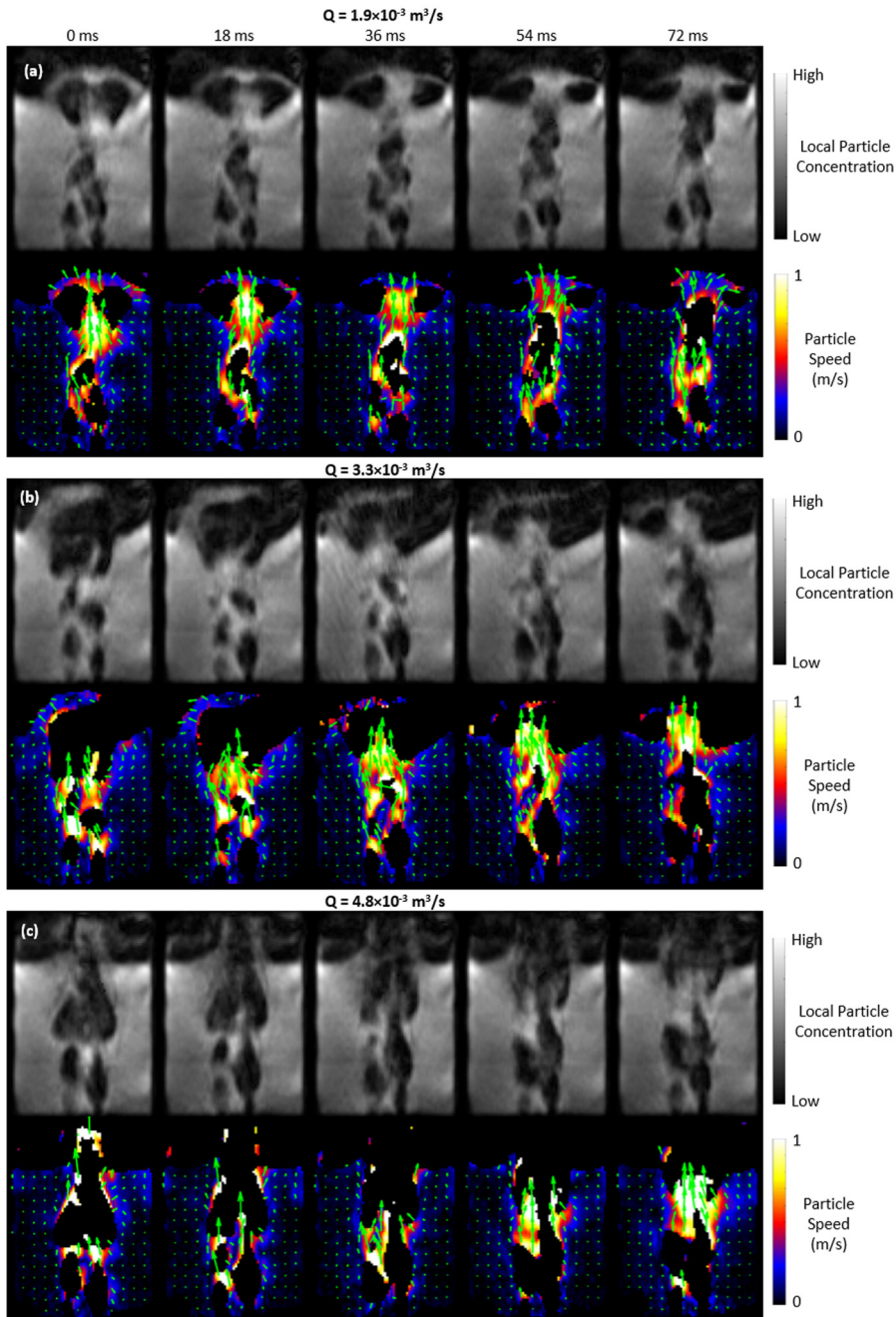
FIG. 2. Time series of images of particle concentration (upper row) and particle velocity (lower row) of a central vertical slice through the bed of two gas jets separated by $d_{\text{sep}}/d_o = 5.0$ injected into an incipiently fluidized bed of 1-mm particles with an average gas velocity through each orifice of $u_{\text{jet}} =$ (a) 38 m/s, (b) 66 m/s, and (c) 97 m/s.
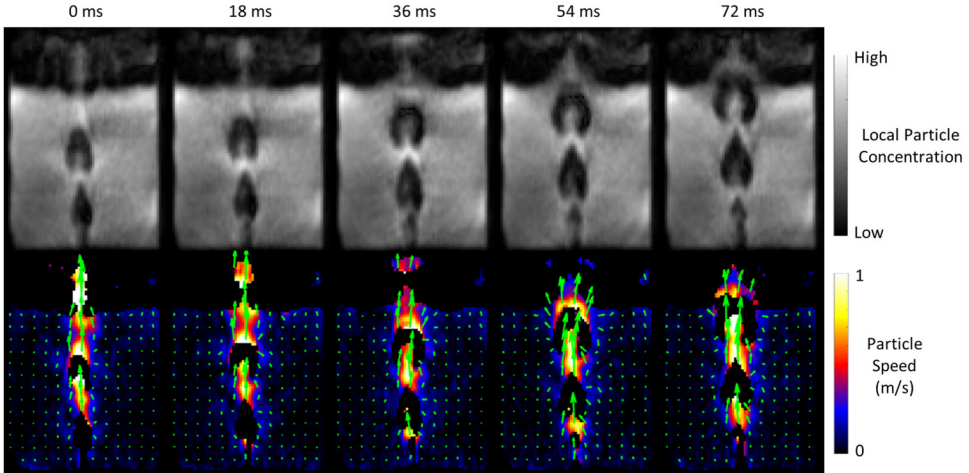
FIG. 3. Time series of images of particle concentration (upper row) and particle velocity (lower row) of a central vertical slice through the bed of a single central jet injected into an incipiently fluidized bed of 1-mm particles with an average gas velocity through the orifice of $u_{\text{jet}} = 52 \, \text{m/s}$.

bubbles and jets. This figure is representative of results from a wider range of flow rates studied; images of experiments at different flow rates are excluded for brevity.

Figure 4 shows a time series of images of particle concentration and velocity for jets separated by $d_{\text{sep}}/d_o = 10.1$ injected into an incipiently fluidized bed of 1-mm particles with $u_{\text{jet}} = 38 \, \text{m/s}$. The jets are not vertical, but rather angled out toward the walls. The jets undulate in width while generally increasing in width with increasing distance above the orifice. Bubbles pinch off from the top of the jets and rise to the bed surface. Particle velocities are fast and upward in the regions directly above and below bubbles and jets and are downward and slow in the region between the two jets as well as the regions between the jets and the walls. Unlike the asynchronous bubble pattern for the
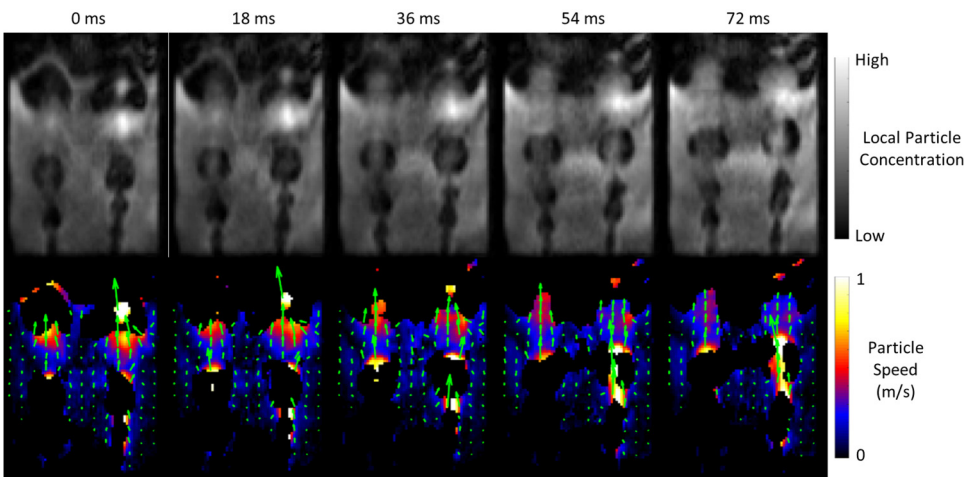

FIG. 4. Time series of images of particle concentration (upper row) and particle velocity (lower row) of a central vertical slice through the bed of two gas jets separated by $d_{\text{sep}}/d_o = 10.1$ injected into an incipiently fluidized bed of 1-mm particles with an average gas velocity through each orifice of $u_{\text{jet}} = 38 \, \text{m/s}$.
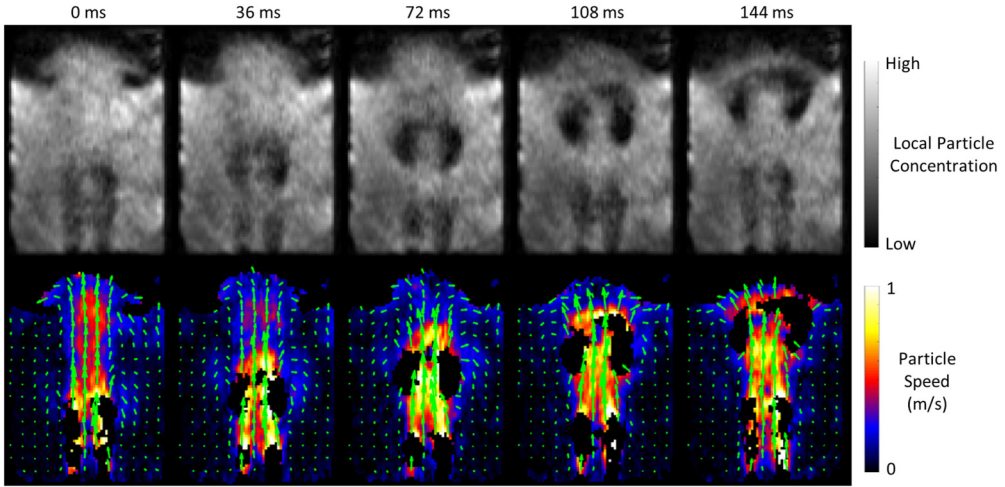
FIG. 5. Time series of images of particle concentration (upper row) and particle velocity (lower row) of a central vertical slice through the bed of two gas jets separated by $d_{\mathrm{sep}}/d_o = 5.0$ injected into an incipiently fluidized bed of 3-mm particles with an average gas velocity through each orifice of $u_{\mathrm{jet}} = 97\,\mathrm{m/s}$.

$d_{\mathrm{sep}}/d_o = 5.0$ separation in Fig. 2, bubbles pinch off from the two jets nearly simultaneously. This figure is representative of results from a wider range of flow rates studied; images of experiments at different flow rates are excluded for brevity.

Figure 5 shows a time series of images for two jets injected into an incipiently fluidized bed of 3-mm particles with a separation distance of $d_{\mathrm{sep}}/d_o = 5.0$ and $u_{\mathrm{jet}} = 97\,\mathrm{m/s}$. Vertical jets form directly above the orifices, and bubbles pinch off from the tops of these jets and rise to the bed surface. Unlike the asynchronous bubble pattern in Fig. 2, the bubbles pinch off simultaneously from the top of each jet. The distinction in particle concentration between the jets and the surrounding particulate phase is less clear than in the corresponding case for 1-mm particles in Fig. 2(a). Particle velocities are fast and upward in the regions directly above and below the bubbles and are slow and downward in the outer annulus of the bed. This figure is representative of results from a wider range of flow rates studied; images of experiments at different flow rates are excluded for brevity.

B. Simulation results

Figure 6 shows time series of images of (a), (b) MRI results and (c), (d) CFD-DEM predictions for closely spaced jets in the 1 mm particle system, showing (a), (c) local particle concentration, and (b), (d) horizontal particle velocity. Results show that CFD-DEM simulations can reproduce the asynchronous, out-of-phase bubble pinch-off phenomenon observed in MRI, providing confidence in the accuracy of the simulations, in addition to a wide array of studies which have shown that CFD-DEM predictions compare well with experimental results [32–36]. Further, both MRI and simulations show that when a bubble is pinching off, particles surrounding the jet move horizontally toward the center of the jet at the point of pinch-off, causing the bubble to pinch off. In contrast, both MRI and simulations show that when a jet is growing, particles move horizontally away from jet, so that the jet can widen.

Figure 7 shows time series of images from the same CFD-DEM simulation as in Fig. 6, showing 3D renderings of the void regions near the jet injection ports (gray), providing (a) a front view and (b) a top view. Results show that there is no significant motion of jets and bubbles out of the central vertical slice shown in Fig. 6.

Figure 8 shows time series of images from the same CFD-DEM simulation as in Fig. 6, but this time showing (a) particle concentration, (b) horizontal gas velocity, (c) horizontal drag force on
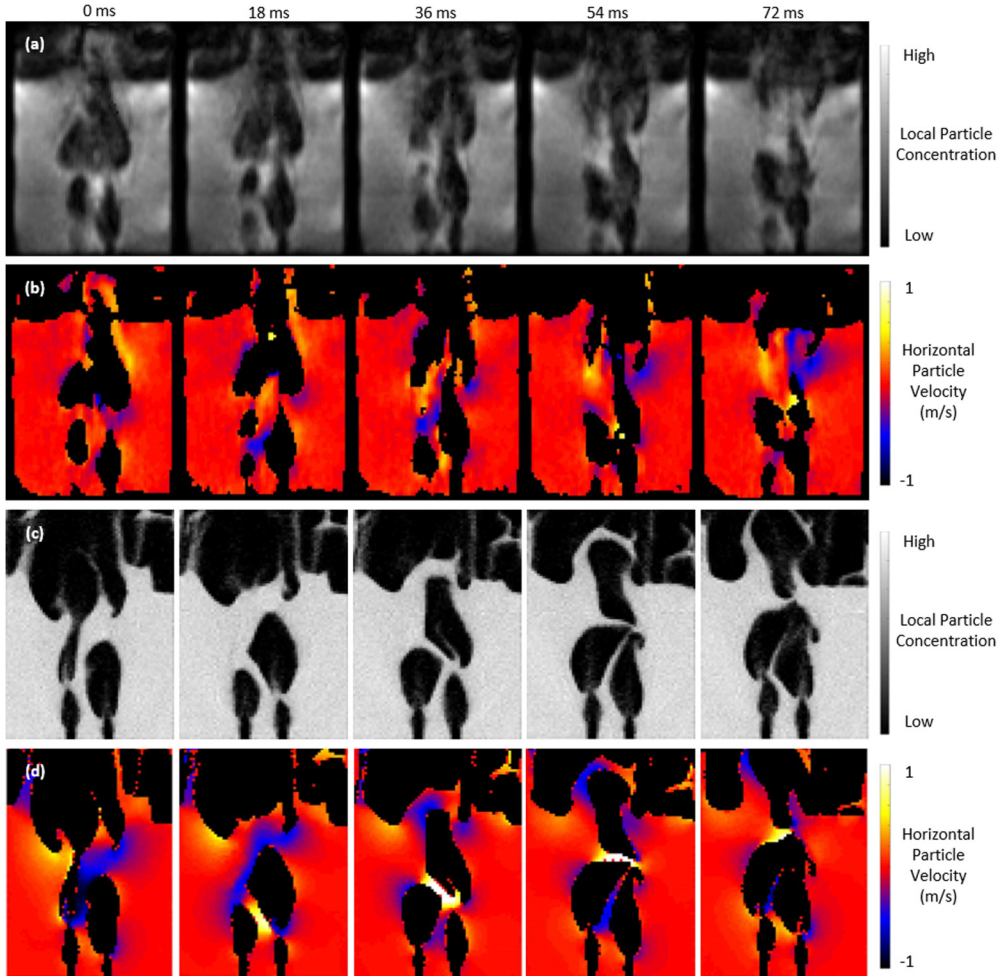
FIG. 6. Time series of images of jet interaction in 1-mm particles showing particle concentration (a), (c) and horizontal particle velocity (b), (d) from MRI measurements (a), (b) and CFD-DEM simulations (c), (d). MRI Jet velocity: 97 m/s; CFD-DEM jet velocity: 3 m/s.

particles, and (d) horizontal particle velocity. In Figs. 8(a), 8(b), and 8(d) void regions are colored black to highlight only results in particle-laden regions, while in Fig. 8(c) void regions are colored white. Results show that the gas velocity in the horizontal direction is highest towards the top of jets with gas moving horizontally away from the jets. This gas velocity leads to high horizontal drag forces on the particles relative to their weight in these regions, pushing the particles away from the tops of jets growing jets. This leads to a pattern in which the drag force acting on central particles between the two jets push particles away from a growing jet and toward a jet which is pinching off. The results for the horizontal particle velocity are similar to those for the drag force: particles move away from the tops of growing jets, causing central particles between the two jets to move away from the growing jet and towards a jet which is pinching off.

Figure 9 shows time series of images of MRI experiments and simulations with jet separation distances corresponding to those in Fig. 6, but with 3-mm fluidized particles. In contrast to the jets in Fig. 6, bubbles pinch of nearly simultaneously, i.e. in-phase, with one another. Figure 9 shows that CFD-DEM simulations can reproduce the simultaneous bubble pinch-off seen experimentally,
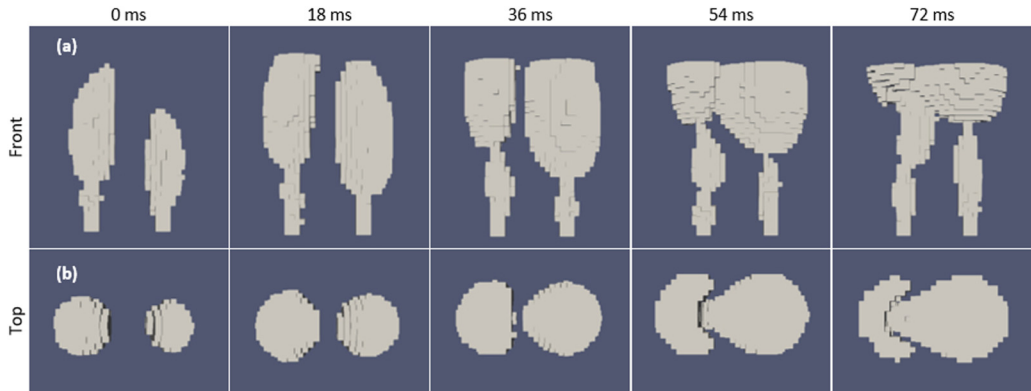
FIG. 7. Time series of images of jet interaction in 1-mm particles from CFD-DEM simulations showing 3D renderings of voids near the orifices from (a) a front view and (b) a top view.
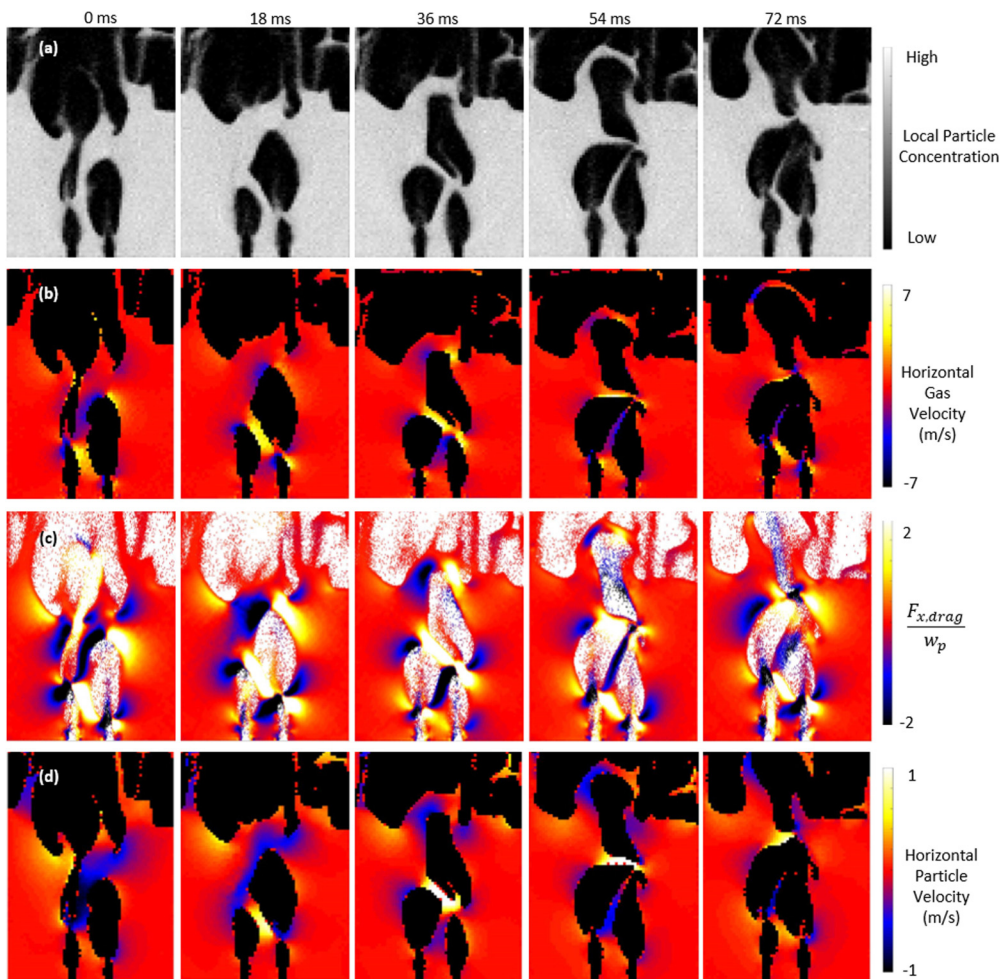

FIG. 8. Time series of images of jet interaction in 1-mm particles from CFD-DEM simulations showing (a) particle concentration, (b) horizontal gas velocity, (c) horizontal drag force normalized by particle weight, and (d) horizontal particle velocity. Jet velocity: 3 m/s.
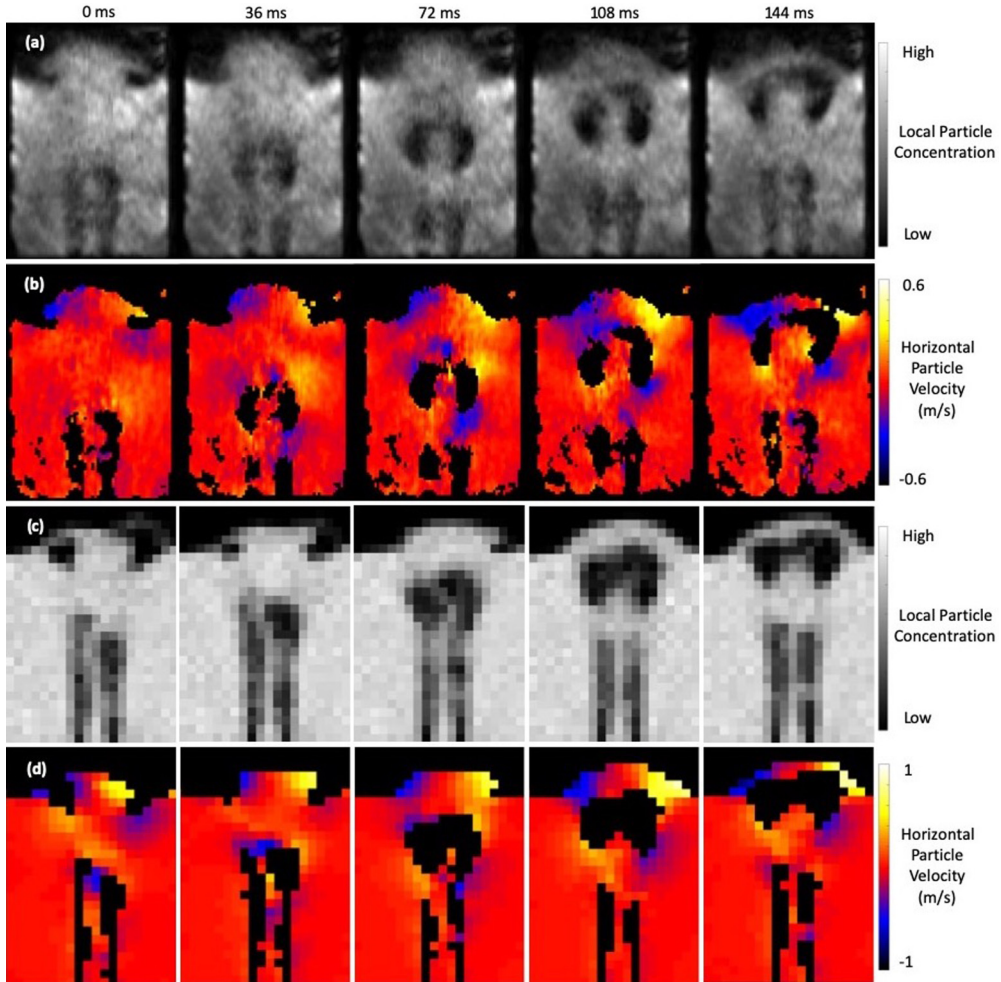
FIG. 9. Time series of images of jet interaction in 3-mm particles showing particle concentration (a), (c) and horizontal particle velocity (b), (d) from MRI measurements (a), (b) and CFD-DEM simulations (c), (d). MRI Jet velocity: 97 m/s; CFD-DEM jet velocity: 40 m/s.

providing further confidence in the predictive capabilities of the simulations. Horizontal particle velocities have lower magnitudes than those observed in Fig. 6, but both Figs. 6 and 9 show that particle velocities move horizontally toward the center of a jet at the point of pinch-off as a bubble pinches off from the jet.

Figure 10 shows the same time series of images as in Fig. 9, but with 3-mm particles instead of 1-mm particles. CFD-DEM predictions show comparable horizontal gas velocity magnitudes to those seen in for 1-mm particles in Fig. 8. In both 3- and 1-mm particles, gas flow moves horizontally away from the tops of growing jets and towards the center of jets at the point of bubble pinch-off. The magnitude of the drag force normalized by particle weight is much smaller in the 3-mm particles than the 1-mm particles. In both 3- and 1-mm particles, drag force pushes particles horizontally away from the tops of growing jets and horizontally toward the point of bubble pinch-off when a jet is pinching off. As with the 1-mm particles, the horizontal particle velocity of particles matches the trends seen in the horizontal drag force; however, the magnitude of horizontal particle velocities in 3-mm particles is significantly lower than that observed in 3-mm particles.
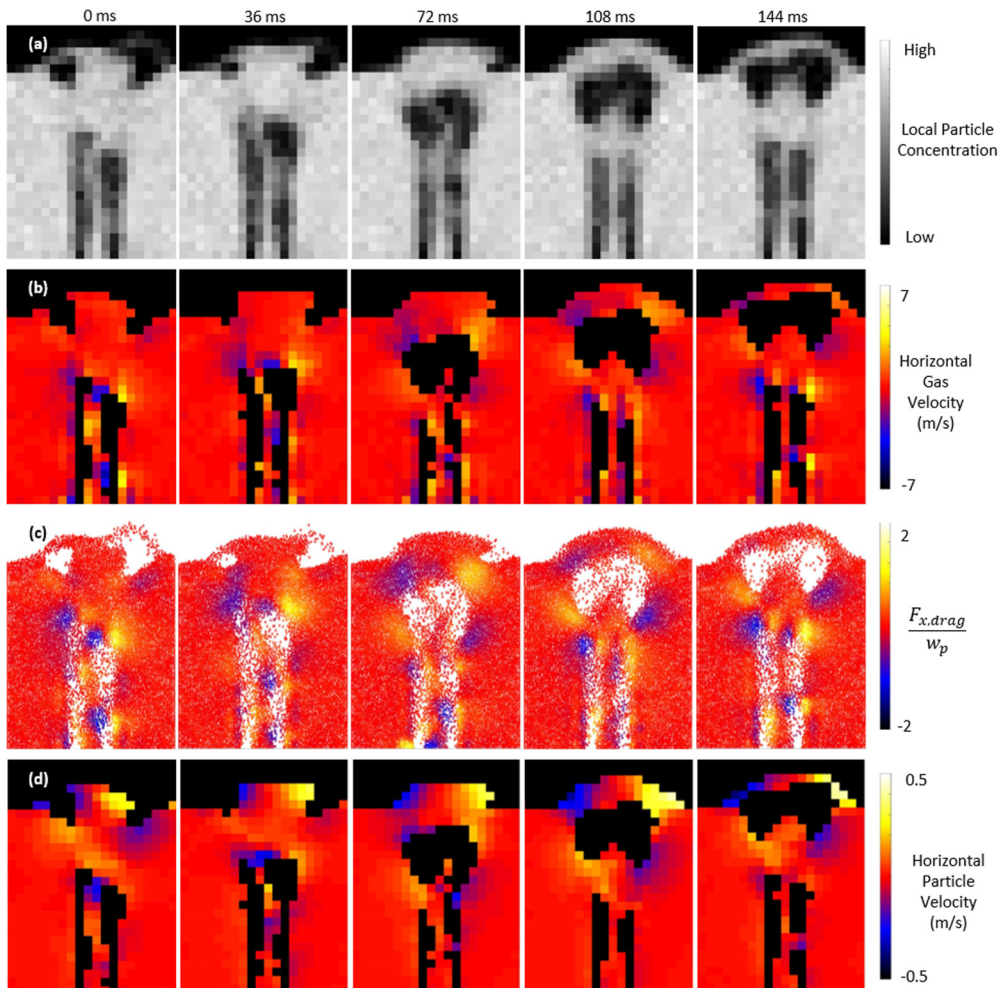
FIG. 10. Time series of images of jet interaction in 3-mm particles from CFD-DEM simulations showing (a) particle concentration, (b) horizontal gas velocity, (c) horizontal drag force normalized by particle weight, and (d) horizontal particle velocity. Jet velocity: 40 m/s.

IV. DISCUSSION

A. Proposed mechanism for asynchronous, out-of-phase bubble pinch-off

The collective MRI and CFD-DEM results lead us to the following mechanism to explain the transition from synchronous to asynchronous bubble pinch-off in the transition regime for jet interaction in fluidized beds: The transition is controlled by the collective horizontal motion of particles in between the two jets, which is dictated by the balance between inertia induced by drag and the momentum dissipation due to interparticle forces. In the synchronous pinch-off regime, drag forces push central particles away from the top of jets, but the particle inertia is dissipated by normal contact forces between particles as they compress into a more densely packed state and frictional forces as particles shear past one another. Thus, drag force pushes central particles near the left jet to the right and central particles near the right jet to the left, yet overall this leads to central particles shearing minimally and compressing, rather than having a net motion to the right or the left. At a critical magnitude of drag force, the inertia imparted on the particles will overcome the dissipative
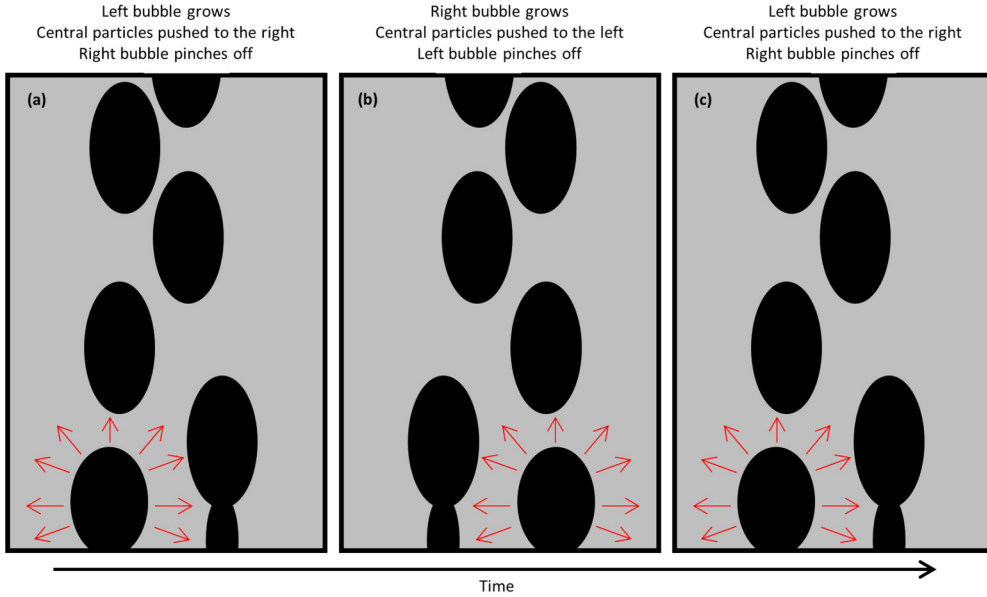
FIG. 11. Schematic of the mechanism underlying the alternating asynchronous bubbling pattern. Red arrows indicate the motion of particles.

forces, causing strong shearing in the particles. Under these conditions, regions of particles where drag forces to the left are slightly stronger than those to the right will move collectively to the left and vice versa. Collective motion of particles to the left will cause the left jet to pinch-off, while collective motion to the right will cause the right bubble to pinch off. Thus, the asynchronous, out-of-phase bubble pinch-off regime is the manifestation of a hydrodynamic instability arising when the drag force acting on the central particles exceeds dissipative interparticle forces due to compression and minor shearing of the central particles, causing the motion of the central particles to become unstable.

This unstable motion of central particles between the two jets leading to the asynchronous, alternating bubble pinch-off phenomenon is shown schematically in Fig. 11. In Fig. 11(a), the left jet is growing, causing particles to be pushed away from it, and thus central particles between the two jets move toward the right jet, causing the right jet to pinch off. Subsequently in Fig. 11(b), the right jet grows, causing the central particles to move away from the right jet and toward the left jet, causing the left jet to pinch off. The cycle begins to repeat itself in Fig. 11(c).

The trends for the transition between the two jet interaction regimes shown in the Results section can be explained as follows. Larger particle have a higher permeability to gas flow ($k \propto d_p^3$) [37] and a larger mass than smaller particles. Thus, while the gas velocities and separation distances may be the same as in smaller particles, the larger particles will have a lower drag force normalized by their weight on them. Thus, the particle compression and minor shearing will dissipate the inertia imparted by drag force, explaining the simultaneous bubbling in Figs. 5, 9, and 10. Similarly, even if smaller particles are used, but the separation distance between jets is larger, there is more space for particles to compress and minorly shear between the jets to dissipate inertial momentum from a stronger drag force on particles coming from the jets as compared to the drag force in the larger particles. Thus, there will be enough inertial dissipation to prevent the asynchronous bubble pattern from forming, explaining the simultaneous bubbling in Fig. 3. Only in cases of small particles and small separation distances between jets will the inertial momentum induced by strong drag forces overcome the ability of compressive and frictional forces to dissipate momentum. Thus, the

asynchronous bubble pinch-off instability only manifests with smaller particles and jet separation distances, as shown in Figs. 2, 6, 7, and 8.

B. Comparison with prior work

Altogether, the results indicate that there are two regimes of jet interaction seen here: (1) synchronous bubble pinch-off, which at moderate separation distances involves jets tilting away from one another, and (2) alternating asynchronous bubble pinch-off. Simultaneous pinch-off occurs at high separation distances between jets, high gas permeability (larger particles) and lower gas flow rates. Asynchronous bubble pinch-off occurs at intermediate separation distances between jets, intermediate gas permeability and intermediate gas flow rates. The transition from the simultaneous to the asynchronous bubble pinch-off regime occurs due to the motion of particles pushed away from one jet towards the other due to jet growth becoming strong enough to pinch off the jet from the other orifice. This transition can be attributed to particle inertial forces due to drag over coming dissipative forces due to particle compression and friction.

Previous studies [1,2,6,7] have classified the interaction between two jets into (1) isolated, (2) transition, and (3) coalescing regimes. In these studies, isolated regimes occur when jets are separated by a sufficiently large distance such that each jet behaves like a single isolated jet and the jets do not influence each other in any way. Coalescing regimes refer to a regime where either the jets themselves coalesce [1] or the bubbles which pinch off from the jets coalesce soon after pinch-off [2]. Transition regimes have been characterized as regimes in which bubbles pinch-off simultaneously and the bubbles and jets influence the shape and height of one another but do not coalesce [6,7], as well as regimes that switch randomly between isolated and coalescing regimes [2]. These studies have focused on differentiating the regimes on the basis of separation distance between jets, often normalized by the orifice diameter, and orifice velocity, often nondimensionalized as a Froude number. Here, we identify that the transition regime can be further sub-divided into regimes that have not been described before in the literature, to the best of the authors' knowledge. As seen in Fig. 4 at moderate separation distances, jets can still influence one another by angling away from one another due to the motion patterns of the central particles between bubbles. Additionally, as shown in Figs. 2, 6, 7, and 8, at smaller separation distances, the motion of central particles can lead to the asynchronous bubble patterns where the jets do not merge but have a strong influence on the temporal development of the other jet. This study also introduces the concept that in addition to separation distance and orifice velocity, the permeability of the particles to gas flow can lead to different flow patterns in the transition regime. For instance, using larger particles with a higher permeability causes a transformation from the asynchronous bubble pattern to a transition regime in which both bubbles detach synchronously, as shown in Figs. 5, 8, and 9.

It is also important to consider the appropriate nondimensionalization of variables related to interacting jets shown experimentally here, particularly for the purpose of creating regime maps for interaction behavior with dividing lines given by critical values of dimensionless parameters. Several dimensional analyses have been performed on single jets injected into fluidized beds [38–40], yielding a variety of dimensionless groups deemed critical to this problem, mostly centered around determining a correlation for the dimensionless jet height (h_{jet}/d_o), where h_{jet} is the jet height and d_o is the orifice diameter. For example, Blake $et\ al.$ [38] determined single jet behavior was governed by four dimensionless groups: Froude number (Fr $= \frac{u_{\mathrm{jet}}^2}{gd_o}$), Reynolds number (Re $= \frac{\rho_g u_{\mathrm{jet}} d_p}{\mu}$), Stokes number (St $= \frac{\rho_s u_{\mathrm{jet}} d_p^2}{\mu d_o}$), and density ratio ($\frac{\rho_g}{\rho_s}$), where g is the acceleration due to gravity, ρ_g is the gas density, ρ_p is the particle density, μ is the gas viscosity, and d_p is the particle diameter. Other studies have found utilized other dimensionless parameters, such as a ratio of densities and diameters ($\frac{\rho_g d_o}{\rho_s d_p}$) [40] and a two-phase Froude number (Fr$_2 = (\frac{\rho_p u_{\mathrm{jet}}^2}{(\rho_p - \rho_f) g d_o})^{1/2}$) [39].

For two interacting jets, all studies [2,6,7,41] have found the separation distance between jets normalized by the orifice diameter (d_{sep}/d_o) to be a critical parameter for characterizing jet interaction and normalized jet height. However, there is some discrepancy as to whether the separation distance between the center of jet orifices (d_{sep}) [2,6], or the separation distance between the closest points of the two orifices to one another ($d_{sep}-d_o$) [7] should be used in the numerator. Guo *et al.* [2] mapped interaction regimes based on Fr$_2$ and d_{sep}/d_o, finding interaction to be dictated largely by the latter parameter, with jet interaction occurring at values of $d_{sep}/d_o < 6$. A different study by Guo *et al.* [41] also included Re as relevant to the dimensionless jet height for two interacting jets. A further study by Guo *et al.* [42] investigated the effect of jet gas velocity on interaction regimes. Zhang *et al.* [6] mapped interaction regimes based on d_{sep}/d_o as well as a dimensional a posteriori parameter, jet height (h_{jet}), finding a significant dependence on both for regime demarcations.

For the system studied here, it is clear that dimensionless separation distance is a critical parameter for determining jet interaction, since the asynchronous alternating bubble pattern does not occur at $d_{sep}/d_o = 10.1$, but does occur at $d_{sep}/d_o = 5.0$ for the 1-mm particles. It is unclear with the current dataset if jet velocity plays a role in determining if the jets will form the asynchronous bubble regime because for all jet velocities studied, the asynchronous jet pattern was observed at $d_{sep}/d_o = 5.0$ for but not at $d_{sep}/d_o = 10.1$ for 1-mm particles. However, the authors anticipate that jet velocities outside the range of those studied here, especially for $5 < d_{sep}/d_o < 10$ could play a role in the formation of the asynchronous pattern. The authors leave it to further study with a larger dataset to determine whether or not u_{jet} is a critical parameter for the regime map, and if so, whether the critical dimensionless parameter is Re, St, Fr, or something else. Such a study could be conducted through numerical; however, the CFD-DEM studies used to the determine the mechanism here are too computationally expensive for a parametric study. Further, it is clear that the particle diameter plays a role in determining the regime of jet interaction, since no asynchronous bubble pattern is observed in the 3-mm particles at $d_{sep}/d_o = 5.0$. The authors expect an appropriate dimensionless group capturing this effect of particle diameter must incorporate differences in gas permeability with particle size [37], since the higher permeability to gas flow in the 3-mm particles is reasoned to be the cause for not observing the asynchronous bubble regime in these particles. The authors defer more definitive assertions on the exact dimensionless groups governing the regimes of jet interaction and the exact dividing lines for the regime maps to future studies in which a wider dataset is available.

The identification of the alternating asynchronous bubble pattern in interacting jets in fluidized beds opens the question of whether or not an equivalent phenomenon exists in gas-liquid systems. The governing physics of gas jets in liquid systems clearly differs from that of gas jets in a gas-solid system, since gas jets in a liquid involve surface tension as well and gas cannot travel freely across the interface between void and liquid-like regions. However, gas-liquid and gas-solid systems have similarities in balances between inertial and dissipative forces influencing their dynamics. Several studies have investigated the interaction of two gas jets injected into a liquid [43–47]. Ruzicka *et al.* [43] identified regimes of interaction involving (i) bubbles forming and pinching off simultaneously, (ii) an "alternating" pattern in which bubbles form and pinch off at one jet for a period of time and then for another period bubbles form and pinch off at the other jet and (iii) bubbles forming and pinching off asynchronously (although not necessarily completely out-of-phase with one another). These studies have often attributed pattern formation to pressure dynamics upstream of the jet injection ports, since most studies involve gas supply from the same plenum chamber [43–45]. However, some studies have involved gas supply from two separate gas lines [46,47], as conducted here. Studies have also attributed the transition from simultaneous to asynchronous bubbling to changes in the motion of liquid surrounding the jets [44,46], similar to the mechanism proposed here. However, the authors are unaware of prior gas-liquid jet interaction studies which have identified and characterized a jetting regime with bubbles pinching off completely out-of-phase from one another.

V. CONCLUSIONS

Rapid magnetic resonance imaging shows that two previously unidentified regimes of jet interaction in fluidized beds exist between the extreme regimes of isolation and coalescence. These regimes are (1) jets angling away from one another at longer separation distances and (2) jets forming an alternating asynchronous bubble pattern at shorter separation distance. The pinch-off of bubbles transitions from being synchronous to asynchronous (and nearly completely out-of-phase) as the separation distance is decreased and particle size is decreased. CFD-DEM simulations and MRI measurements demonstrate that the horizontal motion of particles between the two jets causes the transition from synchronous to asynchronous bubble pinch-off. In the asynchronous, alternating bubble pinch-off regime, particles move away from one jet as it grows, causing the other jet to pinch off. Based on CFD-DEM simulations, we explain this alternating asynchronous jet pinch-off as the manifestation of a hydrodynamic instability which occurs when inertial forces acting on particles due to drag exceed the dissipative forces from particle compression and friction, causing an unstable collective motion of the central particles. This mechanism is similar to that put forward previously for asynchronous bubbling in gas jets in liquid systems [44]; however, we are unaware of prior reports of completely out-of-phase bubble pinch-off in gas-liquid systems.

---

[1] C.-S. Wu and W. B. Whiting, Interacting jets in a fluidized bed, Chem. Eng. Commun. **73**, 1 (1988).

[2] Q. Guo, Z. Tang, G. Yue, Z. Liu, and J. Zhang, Flow pattern transition in a large jetting fluidized bed with double nozzles, AIChE J. **47**, 1309 (2001).

[3] M. S. van Buijtenen, W.-J. van Dijk, N. G. Deen, J. A. M. Kuipers, T. Leadbeater, and D. J. Parker, Numerical and experimental study on multiple-spout fluidized beds, Chem. Eng. Sci. **66**, 2368 (2011).

[4] P. Philippe and M. Badiane, Localized fluidization in a granular medium, Phys. Rev. E **87**, 042206 (2013).

[5] J. Ngoma, P. Philippe, S. Bonelli, J. Y. Delenne, F. Radjai, K. Soga, K. Kumar, G. Biscontin, and M. Kuo, Interaction between two localized fluidization cavities in granular media: Experiments and numerical simulation, in Proceedings of the Geomechanics From Micro to Macro (2015).

[6] K. Zhang, P. Pei, S. Brandani, H. Chen, and Y. Yang, CFD simulation of flow pattern and jet penetration depth in gas-fluidized beds with single and double jets, Chem. Eng. Sci. **68**, 108 (2012).

[7] R. Y. Hong, Q. J. Guo, G. H. Luo, J.-Y. Zhang, and J. Ding, On the jet penetration height in fluidized beds with two vertical jets, Powder Technol. **133**, 216 (2003).

[8] M. Pore, D. J. Holland, T. C. Chandrasekera, C. R. Müller, A. J. Sederman, J. S. Dennis, L. F. Gladden, and J. F. Davidson, Magnetic resonance studies of a gas-solids fluidized bed: Jet-jet and jet-wall interactions, Particuology **8**, 617 (2010).

[9] M. Bieberle, F. Fischer, E. Schleicher, H.-J. Menz, H.-G. Mayer, and U. Hampel, Ultrafast cross-sectional imaging of gas-particle flow in a fluidized bed, AIChE J. **56**, 2221 (2010).

[10] S. Harms, S. Stapf, and B. Blümich, Application of k- and q-space encoding NMR techniques on granular media in a 3D model fluidized bed reactor, J. Magn. Reson. **178**, 308 (2006).

[11] R. Stannarius, Magnetic resonance imaging of granular materials, Rev. Sci. Instrum. **88**, 051806 (2017).

[12] E. Fukushima, Nuclear magnetic resonance imaging as a tool to study flow, Annu. Rev. Fluid Mech. **31**, 95 (1999).

[13] M. Pore, G. H. Ong, C. M. Boyce, M. Materazzi, J. Gargiuli, T. Leadbeater, A. J. Sederman, J. S. Dennis, D. J. Holland, A. Ingram, P. Lettieri, and D. J. Parker, A comparison of magnetic resonance, x-ray, and positron emission particle tracking measurements of a single jet of gas entering a bed of particles, Chem. Eng. Sci. **122**, 210 (2015).

[14] A. C. Rees, J. F. Davidson, J. S. Dennis, P. S Fennell, L. F. Gladden, A. N. Hayhurst, M. D. Mantle, C. R. Müller, and A. J. Sederman, The nature of the flow just above the perforated plate distributor of a gas-fluidized bed, as imaged using magnetic resonance, Chem. Eng. Sci. **61**, 6002 (2006).

[15] C. R. Müller, D. J. Holland, J. F. Davidson, J. S. Dennis, L. F. Gladden, A. N. Hayhurst, M. D. Mantle, and A. J. Sederman, Geometrical and hydrodynamical study of gas jets in packed and fluidized beds using magnetic resonance, Can. J. Chem. Eng. **87**, 517 (2009).

[16] A. Penn, T. Tsuji, D. O. Brunner, C. M. Boyce, K. P. Pruessmann, and C. R. Müller, Real-time probing of granular dynamics with magnetic resonance, Sci. Adv. **3**, e1701879 (2017).

[17] C. M. Boyce, A. Penn, K. P. Pruessmann, and C. R. Müller, Magnetic resonance imaging of gas-solid fluidization with liquid bridging, AIChE J. **64**, 2958 (2018).

[18] A. Penn, C. M. Boyce, T. Kovar, T. Tsuji, K. P. Pruessmann, and C. R. Müller, Real-Time magnetic resonance imaging of bubble behavior and particle velocity in fluidized beds, Ind. Eng. Chem. Res. **57**, 9674 (2018).

[19] C. M. Boyce, A. Penn, A. Padash, M. Lehnert, K. P. Pruessmann, and C. R. Müller, Anomalous collapse of interacting bubbles in a fluidized bed: A magnetic resonance imaging study, Phys. Rev. Fluids **4**, 034303 (2019).

[20] C. M. Boyce, A. Penn, M. Lehnert, K. P. Pruessmann, and C. R. Müller, Characteristics of a single jet injected into an incipiently fluidized bed: A magnetic resonance imaging study, Adv. Powder Technol. **30**, 3146 (2019).

[21] A. Penn, C. M. Boyce, K. P. Pruessmann, and C. R. Müller, Regimes of jetting and bubbling in a fluidized bed studied using real-time magnetic resonance imaging, Chem. Eng. J. **383**, 123185 (2019).

[22] D. Geldart, Types of gas fluidization, Powder Technol. **7**, 285 (1973).

[23] M. K. Stehling, R. Turner, and P. Mansfield, Echo-Planar imaging: Magnetic resonance imaging in a fraction of a second, Science **254**, 43 (1991).

[24] P. T. Callaghan, *Principles of Nuclear Magnetic Resonance Microscopy* (Oxford University Press, Oxford, 1991).

[25] C. Goniva, C. Kloss, N. G. Deen, J. A. M. Kuipers, and S. Pirker, Influence of rolling friction on single spout fluidized bed simulation, Particuology **10**, 582 (2012).

[26] H. G. Weller, G. Tabor, H. Jasak, and C. Fureby, A tensorial approach to computational continuum mechanics using object-oriented techniques, Comput. Phys. **12**, 620 (1998).

[27] C. Kloss, C. Goniva, A. Hager, S. Amberger, and S. Pirker, Models, algorithms and validation for opensource DEM and CFD-DEM, Prog. Comput. Fluid Dyn. Int. J. **12**, 140 (2012).

[28] C. M. Boyce, A. Ozel, N. P. Rice, G. J. Rubinstein, D. J. Holland, and S. Sundaresan, Effective particle diameters for simulating fluidization of nonspherical particles: CFD-DEM models vs. MRI measurements, AIChE J. **63**, 2555 (2017).

[29] C. M. Boyce, D. J. Holland, S. A. Scott, and J. S. Dennis, Limitations on fluid grid sizing for using volume-averaged fluid equations in discrete element models of fluidized beds, Ind. Eng. Chem. Res. **54**, 10684 (2015).

[30] C. Y. Wen and Y. H. Yu, A generalized method for predicting the minimum fluidization velocity, AIChE J. **12**, 610 (1966).

[31] A. Padash and C. M. Boyce, Collapse of a bubble injected side-by-side with another bubble into an incipiently fluidized bed: A CFD-DEM study, Phys. Rev. Fluids **5**, 034304 (2020).

[32] C. M. Boyce, N. P. Rice, A. Ozel, J. F. Davidson, A. J. Sederman, L. F. Gladden, S. Sundaresan, J. S. Dennis, and D. J. Holland, Magnetic resonance characterization of coupled gas and particle dynamics in a bubbling fluidized bed, Phys. Rev. Fluids **1**, 074201 (2016).

[33] C. R. Müller, D. J. Holland, A. J. Sederman, S. A. Scott, J. S. Dennis, and L. F. Gladden, Granular temperature: Comparison of Magnetic Resonance measurements with Discrete Element Model simulations, Powder Technol. **184**, 241 (2008).

[34] C. M. Boyce, D. J. Holland, S. A. Scott, and J. S. Dennis, Adapting data processing to compare model and experiment accurately: A discrete element model and magnetic resonance measurements of a 3D cylindrical fluidized bed, Ind. Eng. Chem. Res. **52**, 18085 (2013).

[35] J. M. Link, W. Godlieb, P. Tripp, N. G. Deen, S. Heinrich, J. A. M. Kuipers, M. Schönherr, and M. Peglow, Comparison of fibre optical measurements and discrete element simulations for the study of granulation in a spout fluidized bed, Powder Technol. **189**, 202 (2009).

[36] Y. Q. Feng and A. B. Yu, Assessment of model formulations in the discrete particle simulation of gas−solid flow, Ind. Eng. Chem. Res. **43**, 8378 (2004).

[37] J. Kozeny, Ueber kapillare Leitung des Wassers im Boden (About capillaries conducting water in the soil), Sitzungsberichte der Akademie der Wissenschaften, Wien, **136**, 271 (1927).

[38] T. R. Blake, H. Webb, and P. B. Sunderland, The nondimensionalization of equations describing fluidization with application to the correlation of jet penetration height, Chem. Eng. Sci. **45**, 365 (1990).

[39] W.-C. Yang and D. L. Keairns, Estimating the jet penetration depth of multiple vertical grid jets, Ind. Eng. Chem. Fundam. **18**, 317 (1979).

[40] J. M. D. Merry, Penetration of vertical jets into fluidized beds, AIChE J. **21**, 507 (1975).

[41] Q. Guo, Z. Liu, and J. Zhang, Flow characteristics in a large jetting fluidized bed with two nozzles, Ind. Eng. Chem. Res. **39**, 746 (2000).

[42] Q. Guo, J. Zhang, and J. Werther, Jetting transition velocity in a jetting fluidized bed with two nozzles, Chem. Eng. J. **92**, 63 (2003).

[43] M. Ruzicka, J. Drahoš, J. Zahradník, and N. H. Thomas, Structure of gas pressure signal at two-orifice bubbling from a common plenum, Chem. Eng. Sci. **55**, 421 (2000).

[44] M. Ruzicka, J. Drahoš, J. Zahradník, and N. H. Thomas, Natural modes of multi-orifice bubbling from a common plenum, Chem. Eng. Sci. **54**, 5223 (1999).

[45] S. Xie and R. B.H. Tan, Bubble formation at multiple orifices—Bubbling synchronicity and frequency, Chem. Eng. Sci. **58**, 4639 (2003).

[46] F. A. C. Pereira, E. Colli, and J. C. Sartorelli, Synchronization of two bubble trains in a viscous fluid: Experiment and numerical simulation, Phys. Rev. E **87**, 022917 (2013).

[47] P. Dzienis, R. Mosdorf, and T. Wyszkowski, Nonlinear dynamics of self-organising bubble departures from twin nozzles, Meccanica **54**, 2119 (2019).